



A satellite-based biosphere parameterization for net ecosystem CO₂ exchange: Vegetation Photosynthesis and Respiration Model (VPRM)

Pathmathevan Mahadevan,¹ Steven C. Wofsy,¹ Daniel M. Matross,^{1,2} Xiangming Xiao,³ Allison L. Dunn,¹ John C. Lin,⁴ Christoph Gerbig,⁵ J. William Munger,¹ Victoria Y. Chow,¹ and Elaine W. Gottlieb¹

Received 4 April 2006; revised 7 August 2007; accepted 12 September 2007; published 12 April 2008.

[1] We present the Vegetation Photosynthesis and Respiration Model (VPRM), a satellite-based assimilation scheme that estimates hourly values of Net Ecosystem Exchange (NEE) of CO₂ for 12 North American biomes using the Enhanced Vegetation Index (EVI) and Land Surface Water Index (LSWI), derived from reflectance data of the Moderate Resolution Imaging Spectroradiometer (MODIS), plus high-resolution data for sunlight and air temperature. The motivation is to provide reliable, fine-grained first-guess fields of surface CO₂ fluxes for application in inverse models at continental and smaller scales. An extremely simple mathematical structure, with minimal numbers of parameters, facilitates optimization using in situ data, with finesse provided by maximal infusion of observed NEE and environmental data from networks of eddy covariance towers across North America (AmeriFlux and Fluxnet Canada). Cross validation showed that the VPRM has strong prediction ability for hourly to monthly timescales for sites with similar vegetation. The VPRM also provides consistent partitioning of NEE into Gross Ecosystem Exchange (GEE, the light-dependent part of NEE) and ecosystem respiration (*R*, the light-independent part), half-saturation irradiance of ecosystem photosynthesis, and annual sum of NEE at all eddy flux sites for which it is optimized. The capability to provide reliable patterns of surface flux for fine-scale inversions is presently limited by the number of vegetation classes for which NEE can be constrained by the current network of eddy flux sites and by the accuracy of MODIS data and data for sunlight.

Citation: Mahadevan, P., S. C. Wofsy, D. M. Matross, X. Xiao, A. L. Dunn, J. C. Lin, C. Gerbig, J. W. Munger, V. Y. Chow, and E. W. Gottlieb (2008), A satellite-based biosphere parameterization for net ecosystem CO₂ exchange: Vegetation Photosynthesis and Respiration Model (VPRM), *Global Biogeochem. Cycles*, 22, GB2005, doi:10.1029/2006GB002735.

1. Introduction

[2] A primary goal of studying the terrestrial carbon cycle is to determine the magnitude of Net Ecosystem Exchange (NEE) of carbon dioxide between the terrestrial biosphere and the atmosphere and to understand the main drivers for hourly, seasonal, and interannual variations of NEE [Wofsy and Harriss, 2002]. Particular interest attaches to time-

resolved measurements of fluxes on regional and continental scales, too small to be reliably resolved by global inverse models, but too large for direct measurement.

[3] Inverse (“top down”) analyses of CO₂ budgets on regional scales utilize measurements of atmospheric CO₂ concentrations on towers and by aircraft within the regions where sources and sinks are most active [Tans, 1980; Fung, 1993; Tans *et al.*, 1993; Bakwin *et al.*, 1998; Lin *et al.*, 2004; Gerbig *et al.*, 2005]. These data are influenced by small-scale, near-field fluxes as well as by continental and global sources and sinks, and the analysis therefore requires fine-scale spatial and temporal resolution for both transport fields and for distributions of surface fluxes [Gerbig *et al.* 2003a, 2003b; Baker *et al.*, 2006]. Fluxes must be resolved on timescales including hourly, seasonal, and annual and on spatial scales as small as 1–10 km, a difficult challenge because NEE represents the difference between uptake (photosynthesis) and loss (respiration) processes that vary on a wide range of timescales [Goulden *et al.*, 1996; Katul *et al.*, 2001].

¹Department of Earth and Planetary Science and Division of Applied Science and Engineering, Harvard University, Cambridge, Massachusetts, USA.

²Now at Department of Environmental Science, Policy, and Management, University of California, Berkeley, Berkeley, California, USA.

³Complex Systems Research Center, Institute for the Study of Earth, Oceans, and Space, University of New Hampshire, Durham, New Hampshire, USA.

⁴Department of Earth and Environmental Sciences, University of Waterloo, Waterloo, Ontario, Canada.

⁵Max-Planck-Institut für Biogeochemie, Jena, Germany.

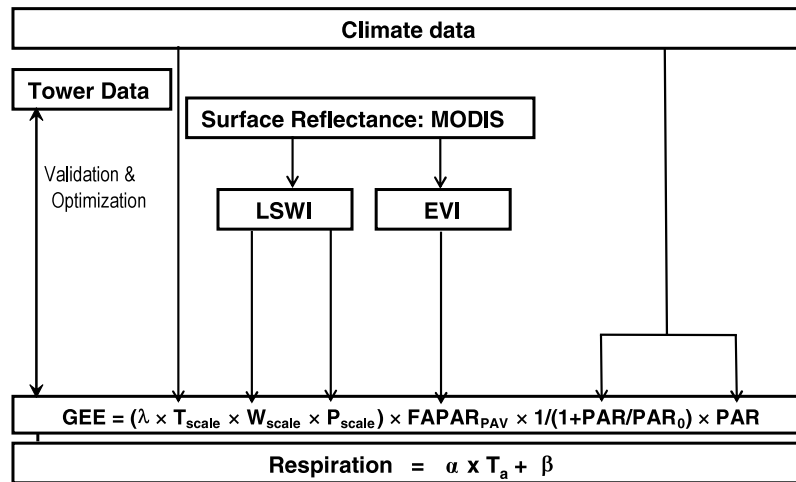


Figure 1. Schematic diagram of the Vegetation Photosynthesis Respiration Model (VPRM). EVI: Enhanced Vegetation Index; LSWI: Land Surface Water Index; $FAPAR_{PAV}$: the fraction of incident light absorbed by the photosynthetically active vegetation in the canopy; T_{scale} , P_{scale} , and W_{scale} : scalars for temperature, leaf phenology, and canopy water content, respectively. Gross Ecosystem Exchange (GEE) is the light-dependent part of Net Ecosystem Exchange (NEE), and Respiration (R) is the light-independent part. MODIS refers to the Moderate Resolution Imaging Spectroradiometer onboard the NASA Terra and Aqua satellites; PAR_0 , λ , α , and β are the four model parameters, one set per vegetation type.

[4] Since the inception of inverse modeling of CO_2 , it has been recognized that surface flux submodels must accurately represent relevant spatiotemporal variations of NEE [Fung *et al.*, 1987; Ruimy *et al.*, 1995; Sellers *et al.*, 1996; Goetz and Prince, 1999; Xiao *et al.*, 2002, 2004a, 2004b]. A priori surface flux models must have a low order of parameterization, so that the optimization process is well constrained [Denning *et al.*, 1995; Lin *et al.*, 2004], while retaining the required fine spatial and temporal resolution.

[5] The present paper addresses the need to reliably represent surface fluxes at fine time/space scales with minimal parameters, into which we infuse the maximum information from observations. We use remotely sensed data to define vegetation properties with fine spatial resolution. Unfortunately, temporal resolution is poor, and direct information on NEE is lacking. We use measurements of NEE from eddy flux towers [Baldocchi *et al.*, 2001] for direct flux data at high temporal resolution, capturing ecosystem functional responses to the environment at sites in North, Central, and South America, but, unfortunately, only small spatial scales (1 km^2).

[6] The Vegetation Photosynthesis Respiration Model (VPRM) presented here assimilates remote sensing, meteorological, and tower flux data for a large number of sites in order to represent surface fluxes with the highest possible fidelity. Model structure is made very simple to facilitate subsequent inverse analysis. Formulation of the VPRM starts from the Vegetation Photosynthesis Model (VPM) of Xiao *et al.* [2004a, 2004b], which estimates Gross Ecosystem Exchange (GEE) using satellite-based vegetation indices and environmental data, adding respiration (R) to provide NEE and a nonlinear function to account for the response of GEE to light. The Enhanced Vegetation Index (EVI) [Huete

et al., 1997, 2002] estimates of the Fraction of Photosynthetically Active Radiation (PAR) absorbed by photosynthetically active parts of the vegetation ($FAPAR_{PAV}$) [Xiao *et al.*, 2004a, 2004b] and the Land Surface Water Index (LSWI) help capture the effects of water stress and leaf phenology [Xiao *et al.*, 2004a, 2004b], especially for vegetation that becomes dormant in summer (e.g., grasslands).

[7] The VPRM shares many features of earlier models for surface CO_2 fluxes (e.g., NASA-CASA [Potter *et al.*, 1993, 1999], SiB2 [Sellers *et al.*, 1996], and TURC [Lafont *et al.*, 2002]) developed for, and most appropriate to, global-scale inverse analysis, but it returns to the simpler functional representation introduced by Fung *et al.* [1987]. As summarized schematically in Figure 1, the VPRM systematically incorporates data from eddy flux towers, spanning dominant vegetation types over North America, plus MODIS data and high-resolution meteorological fields, to provide a much finer representation of surface fluxes than in previous simple models. VPRM NEE fields are thus optimally consistent with eddy flux data, and the model is readily exported to potential users and optimized using atmospheric data. Inversion of the VPRM is intended to enable it to capture seasonal and spatial variations of NEE not explicitly represented a priori.

2. Model Framework

[8] Monteith [1972] showed that ecosystem production correlates with the Fraction of Absorbed Photosynthetically Active Radiation (FAPAR). FAPAR is often estimated as a linear or nonlinear function of the Normalized Difference Vegetation Index (NDVI) [Prince and Goward, 1995; Running *et al.*, 2000], the normalized ratio between

satellite-derived reflectance in the red (ρ_{red}) and near-infrared (ρ_{nir}) bands [Tucker, 1979],

$$NDVI = \frac{\rho_{nir} - \rho_{red}}{\rho_{nir} + \rho_{red}}, \quad (1)$$

using NDVI from the Advanced Very High Resolution Radiometer (AVHRR) to compute rates of terrestrial photosynthesis [e.g., Fung et al., 1987; Potter et al., 1993].

[9] Recent studies [Xiao, et al., 2004a, 2004b, 2005] showed that MODIS EVI [Huete et al., 1997, 2002] is more closely correlated with photosynthesis [Xiao et al., 2004a, 2004b] across a larger range of leaf area index and more closely follows phenology:

$$EVI = G \times \frac{(\rho_{nir} - \rho_{red})}{\rho_{nir} + (C_1 \times \rho_{red} - C_2 \times \rho_{blue}) + L}, \quad (2)$$

where $G = 2.5$, $C_1 = 6$, $C_2 = 7.5$, and $L = 1$. Inclusion of the blue band helps account for atmospheric contamination, and L helps compensate for soil background reflectance. The VPRM also utilizes the LSWI [Xiao et al., 2004a, 2004b] to help capture effects of water stress and phenology on plant photosynthesis:

$$LSWI = \frac{\rho_{nir} - \rho_{swir}}{\rho_{nir} + \rho_{swir}}, \quad (3)$$

where NIR refers to the 841–876 nm band, and SWIR refers to 1628–1652 nm.

2.1. Gross Ecosystem Exchange

[10] We divide NEE into a light-dependent term, Gross Ecosystem Exchange (GEE), and a light-independent part, ecosystem respiration (R), where $NEE = -GEE + R$, following the sign convention that uptake of CO_2 by plants is a negative flux (removal from the atmosphere). GEE is represented by

$$GEE = \varepsilon \times \frac{1}{(1 + PAR/PAR_0)} \times PAR \times FAPAR_{PAV}, \quad (4)$$

where $FAPAR_{PAV}$ is the Fraction of Photosynthetically Active Radiation (PAR, $\mu\text{mol m}^{-2} \text{s}^{-1}$) absorbed by the photosynthetically active portion of the vegetation (PAV), PAR_0 is the half-saturation value, and ε is the light use efficiency ($\mu\text{mol CO}_2/\mu\text{mol PPF}$) at low light levels. We decompose ε into the product of the maximum quantum yield, ε_0 , and factors ranging between 0 and 1 that reduce light use efficiency,

$$\varepsilon = \varepsilon_0 \times T_{scale} \times W_{scale} \times P_{scale} \quad (5)$$

On average, ε_0 has a value around 1/6 for well-watered, C_3 plants at optimal temperatures.

[11] The parameter T_{scale} in equation (5) represents the temperature sensitivity of photosynthesis, calculated at each time step using the equation developed for the Terrestrial Ecosystem Model [Raich et al., 1991]:

$$T_{scale} = \frac{(T - T_{min})(T - T_{max})}{[(T - T_{min})(T - T_{max}) - (T - T_{opt})^2]}, \quad (6)$$

where T_{min} , T_{max} , and T_{opt} are minimum, maximum, and optimal temperatures ($^{\circ}\text{C}$) for photosynthesis, respectively

[Aber and Federer, 1992; Raich et al., 1991]. If air temperature falls below T_{min} , T_{scale} is set to be zero [Xiao et al., 2004a, 2004b].

[12] Since temperature and PAR are correlated on a daily basis, inclusion of T_{scale} in equation (5) modifies values of PAR_0 inferred from tower flux data. Moreover, were the parameters T_{min} , T_{max} , and T_{opt} in equation (6) to be fit to eddy flux data along with the respiration equation (below) and PAR_0 , parameter values would be unstable because of correlation between the parameters; therefore T_{min} , T_{max} , and T_{opt} were fixed at literature values. The role of T_{scale} in the VPRM is explored in a sensitivity analysis below.

[13] The function P_{scale} accounts for effects of leaf age on canopy photosynthesis, using EVI and LSWI to identify the green-up (leaf expansion) and senescence phases [Xiao et al., 2002, 2004a; Boles et al., 2004]. For evergreen classes, P_{scale} is assumed to be 1 for the whole year. For deciduous vegetation and grasslands we computed P_{scale} as a linear function of LSWI from bud burst to leaf full expansion (“phase 1”) by

$$P_{scale} = \frac{1 + LSWI}{2}. \quad (7)$$

[14] After leaf full expansion (phase two), P_{scale} was set to 1, and equation (7) was adopted again during senescence (phase 3). The dates for the three phases of phenology (bud burst, full canopy, and senescence) were obtained using an EVI seasonal threshold similar to that of the MODIS phenology product MOD12Q2 [Friedl et al., 2003]. Thus for large-scale application of the VPRM across North America, MOD12Q2 dates can be used directly.

[15] The effect of water stress on GEE (W_{scale}) is a complex function of soil moisture and vapor pressure deficit (VPD) [e.g., Field et al., 1995; Running et al., 2000]. Soil moisture is currently used within the VPRM, since it cannot be derived directly from weather or remote sensing data [Pathmathevan et al., 2003]. We explored the use of the soil moisture product from the North American Land Data Assimilation System (NLDAS) [Mitchell et al., 2004], but we found the NLDAS product to be insufficiently accurate in simulating site soil moisture data. VPD could be derived from meteorological data, but it is a relatively minor influence compared to other factors (e.g., soil moisture) for most North American vegetation [cf. Powell et al., 2006; Makela et al., 2006; Cunningham, 2005]. A test run including VPD in the optimization of the VPRM at Harvard Forest produced results indistinguishable from a model where this factor was omitted, in part because of the very strong correlation of VPD with air temperature.

[16] Therefore following Xiao et al. [2004a], we express W_{scale} as

$$W_{scale} = \frac{1 + LSWI}{1 + LSWI_{max}}, \quad (8)$$

where $LSWI_{max}$ is the maximum LSWI within the plant-growing season for each site (or pixel). LSWI has been shown to capture drought-induced changes in plant canopies for ecosystems that senesce during dry periods, such as grasslands, but not for other vegetation. Hence effects of water stress are not explicitly included in the

VPRM and thus represent a principal source of unaccounted variance to be captured in an inverse analysis via adjustments to the VPRM parameters. This should be possible in inverse studies with regional resolution in space and month resolution in time, because soil moisture and related quantities tend to covary on regional scales and to change relatively slowly with time (\sim weeks).

[17] The complete expression for GEE in the VPRM is thus given by

$$\text{GEE} = \lambda \times T_{\text{scale}} \times P_{\text{scale}} \times W_{\text{scale}} \times \text{EVI} \times \frac{1}{(1 + \text{PAR}/\text{PAR}_0)} \times \text{PAR} \quad (9)$$

Here λ replaces ε_0 , in order to aggregate into one parameter empirical adjustments to P_{scale} , T_{scale} , and W_{scale} ; λ and PAR_0 are the only adjustable parameters for description of the light-dependent part of NEE, with values derived below from tower flux data.

[18] PAR is measured at all flux tower sites, but not across the continent. At large scales the VPRM will be driven using shortwave (SW) radiation, available for almost all of North America from Geostationary Operational Environmental Satellite (GOES) data [e.g., *Diak et al.*, 2004] and from assimilated meteorological products. SW is very closely correlated with PAR; $\text{SW} \approx 0.505 \times \text{PAR}$ (units: SW, Watts/m²; PAR, $\mu\text{mole m}^{-2} \text{s}^{-1}$).

2.2. Ecosystem Respiration

[19] Plant and soil respiration rates generally increase as temperatures rise [*Grace and Rayment*, 2000; *Piovesan and Adams*, 2000], and we therefore represented R as

$$R = \alpha \times T + \beta. \quad (10)$$

We set $T = T_{\text{low}}$ in equation (10) when $T \leq T_{\text{low}}$, to account for the persistence of soil respiration in winter, when air temperatures are very cold but soils remain warm. Values for α , β , and T_{low} were derived from tower flux data for each vegetation type (Tables 1 and 2). The intercept in equation (10) can be interpreted biogeochemically as the flux-weighted mean size of the respiring pools of organic matter in the ecosystem. In nature this number is determined by a complex set of antecedent conditions, such as site history and available stocks of necromass, in addition to climate factors. The VPRM adopts the zero-order approximation that these factors are uniform for each vegetation type, because site-specific information is not currently available from remote sensing or land cover databases. This approximation thus represents a second principal source of unaccounted variance, designed to be captured in an inverse analysis via adjustments to the VPRM parameters.

2.3. Net Ecosystem Exchange

[20] The full VPRM model equation is

$$\text{NEE} = -\lambda \times T_{\text{scale}} \times P_{\text{scale}} \times W_{\text{scale}} \times \frac{1}{(1 + \text{PAR}/\text{PAR}_0)} \times \text{EVI} \times \text{PAR} + \alpha \times T + \beta \quad (11)$$

$$\text{NEE} = -\lambda \times T_{\text{scale}} \times P_{\text{scale}} \times W_{\text{scale}} \times \frac{1}{(1 + \text{PAR}/\text{PAR}_0)} \times \text{EVI} \times \text{PAR} + \alpha \times T + \beta \quad (12)$$

adjusted in an inverse model application to provide an accurate representation for the distribution NEE in space and time across North America. The a priori estimates of these parameters are derived by optimizing the model using flux towers data at sites denoted as ‘‘calibration sites’’. We assess transferability across the landscape by examining data from sites not used in deriving the prior estimates (‘‘validation sites’’).

3. Study Sites and Data

3.1. Vegetation and Tower Flux Data

[21] Tower measurements of NEE and water fluxes are made at numerous sites in North America and worldwide [*Baldocchi et al.*, 2001]. We assembled a large subset of these data to calibrate and test VPRM surface fluxes, classified by vegetation type on the basis of the 1-km International Geosphere Biosphere Programme (IGBP) classification [*Belward et al.*, 1999].

[22] Since tower flux data are not available for each of the 17 IGBP vegetation classes, we grouped North American ecosystems into nine major classes for which eddy flux data are available: evergreen forests, deciduous forest, mixed forest, shrubland (including open and closed shrubland), savannas (savannas and woody savannas), cropland, grassland (grassland, cropland/natural vegetation mosaic, and barren or sparsely vegetated), permanent wetlands, and others (especially the water bodies).

[23] Two of these nine large classes needed to be subdivided to account for major biophysical differences within them. The IGBP class ‘‘evergreen needleleaf forests’’ (\sim 6.751% of land area) is broadly distributed, from boreal boggy black spruce to subtropical slash pine. We combined this class with ‘‘evergreen broadleaf forests’’, which have negligible occurrence in North America (\sim 0.5%), and then subdivided into four classes (boreal (e.g., black spruce), wet temperate/montane (e.g., Douglas fir, western white pine), dry temperate (e.g., ponderosa pine), and subtropical (e.g., slash pine, with strong summertime droughts)) by climate zone, using Holdridge Life Zone data [*Monserud and Leemans*, 1992]. Similarly, ‘‘cropland’’ was divided into soy and corn (to be expanded to include wheat when data become available). Fortunately, suitable eddy flux data are available for these subdivisions.

[24] We designated 11 tower sites to calibrate the four parameters for each vegetation class (except water, snow and ice, where fluxes are assumed zero), and identified 11 other sites for testing (‘‘validation’’) as listed in Table 1. More details and data for the 22 test sites can be obtained from network Web sites (<http://public.ornl.gov/ameriflux/> and <http://www.fluxnet-canada.ca/>) and from the original references in Table 1.

[25] The calibration sites for evergreen forests are the Northern Old Black Spruce (NOBS/BOREAS) site in Manitoba (boreal forest), Niwot Ridge in Colorado (subalpine coniferous forest), and Metolius Forest in Oregon

Table 1. Carbon Flux and MODIS Data From These 22 AmeriFlux and Fluxnet-Canada Sites Used in This Study

Abbreviation	Site	Data Year	LAT(N)	LON(W)	Country	Reference
NOBS	NSA old black spruce forest	2000–2003	55.879	98.480	MB, Canada	Goulden <i>et al.</i> [1998], Dunn <i>et al.</i> [2007]
NIWOT	Niwot Ridge Forest (NWT1)	2000–2003	40.033	105.546	Colorado, United States	Monson <i>et al.</i> [2002], Yi <i>et al.</i> [2004]
METOLIUS	Metolius-intermediate (69 years)	2002–2004	44.452	121.557	Oregon, United States	Coops <i>et al.</i> [2005]
DONALDSON	ponderosa pine forest Donaldson midrotation (12 years)	2001–2002	29.755	82.163	Florida, United States	Clark <i>et al.</i> [1999, 2004]
HARVARD	slash pine forest	2000–2003	42.538	72.171	Massachusetts, United States	Wofsy <i>et al.</i> [1993], Davidson <i>et al.</i> [2002a]
HOWLAND	Harvard Forest (main) Howland Forest (main)	2000–2003	45.204	68.740	Maine, United States	Hollinger <i>et al.</i> [1999], Davidson <i>et al.</i> [2002a, 2002b]
LUCKY-HILL	Walnut-Gulch Lucky Hills shrublands	2000–2003	31.744	110.052	Arizona, United States	Emmerich [2003]
TONZI	Tonzi Range savannas	2002–2004	38.432	120.966	California, United States	Xu and Baldocchi [2003], Baldocchi <i>et al.</i> [2004]
MEAD-S2	irrigated maize-soybean rotation	soy: 2002 corn: 2003	41.099	96.281	Nebraska, United States	Verma <i>et al.</i> [2005]
VAIRA	site (site 2) Vaira Range grassland	2001–2003	38.407	120.951	California, United States	Xu and Baldocchi [2004], Baldocchi <i>et al.</i> [2004]
PEATLAND	eastern peatland, permanent wetland	2002	45.409	75.520	Ontario, Canada	Laffleur <i>et al.</i> [2001, 2003]
ANILGRASS	Walnut River watershed, grassland	2002–2003	37.521	96.855	Kansas, United States	Song and Wesely [2003], Song <i>et al.</i> [2006], Coulter <i>et al.</i> [2006]
WLEF	Park Falls/WLEF	2000–2001	45.946	90.272	Wisconsin, United States	Davis <i>et al.</i> [2003]; Wang <i>et al.</i> [2007b]
WCREEK	Willow Creek	2000–2004	45.806	90.080	Wisconsin, United States	Desai <i>et al.</i> [2005] Cook <i>et al.</i> [2004]
LCREEK	Lost Creek	2001–2004	46.083	89.979	Wisconsin, United States	Desai <i>et al.</i> [2008] Wang <i>et al.</i> [2006]
SOBS	SSA old black spruce forest	2000–2004	53.987	105.118	Saskatchewan, Canada	Turner <i>et al.</i> [2003]; Griffiths <i>et al.</i> [2003]
B1850	NSA 1850 burn site	2001–2004	55.880	98.480	Manitoba, Canada	Goulden <i>et al.</i> [2006]
EOBS	Quebec mature boreal forest	2004	49.693	74.342	PQ, Canada	Bergeron <i>et al.</i> [2007]
BOND	Bondville maize-soy cropland	soy: 2000 corn: 2001	40.006	88.292	Illinois, United States	Hollinger <i>et al.</i> [2005], Meyers and Hollinger [2004]
INDIANA	Morgan Monroe State Forest	2000–2003	39.323	86.413	Indiana, United States	Schmid <i>et al.</i> [2000] Su <i>et al.</i> [2004]
DUKE PP	Duke Forest: loblolly pine	2001–2004	35.971	79.093	North Carolina, United States	Oren <i>et al.</i> [2006]
DUKE HW	Duke Forest: hardwoods	2001–2004	35.974	79.100	North Carolina, United States	Stoy <i>et al.</i> [2005]

Table 2. Parameters PAR_0 , λ , α , β , and Their Variances and Light Use Efficiency at Calibration Sites^a

Site	T_{min}	T_{opt}	T_{max}	T_{low}	PAR_0	λ	α	β	$\sigma-PAR_0$	$\sigma-\lambda$	$\sigma-\alpha$	$\sigma-\beta$
HARVARD	0	20	40	5	570	0.127	0.271	0.25	14	0.002	0.006	0.060
HOWLAND	0	20	40	2	629	0.123	0.244	-0.24	17	0.002	0.004	0.036
NOBS	0	20	40	1	262	0.234	0.244	0.14	5	0.004	0.002	0.015
NIWOT	0	20	40	1	446	0.128	0.250	0.17	13	0.003	0.003	0.018
METOLIUS	0	20	40	2	1206	0.097	0.295	-0.43	39	0.002	0.003	0.028
SOY_MEADS2	5	22	40	2	2051	0.064	0.209	0.20	137	0.002	0.005	0.058
CORN_MEAD	5	22	40	2	11250	0.075	0.173	0.82	1746	0.002	0.006	0.081
TONZI	2	20	40	-	3241	0.057	0.012	0.58	293	0.002	0.002	0.036
VAIRA	2	18	40	-	542	0.213	0.028	0.72	23	0.006	0.002	0.035
DONALDSON	0	20	40	1	790	0.114	0.153	1.56	18	0.002	0.004	0.076
LUCKY-HILLS	2	20	40	-	321	0.122	0.028	0.48	14	0.004	0.001	0.019
PEATLAND	0	20	40	3	558	0.051	0.081	0.24	23	0.002	0.002	0.019

^aUnits are as follows: PAR_0 : $\mu\text{mole m}^{-2} \text{s}^{-1}$; λ : $\mu\text{mole CO}_2 \text{ m}^{-2} \text{s}^{-1}/\mu\text{mole PAR m}^{-2} \text{s}^{-1}$; α : $\mu\text{mole CO}_2 \text{ m}^{-2} \text{s}^{-1}/^\circ\text{C}$; β : $\mu\text{mole CO}_2 \text{ m}^{-2} \text{s}^{-1}$. Light use efficiency: λ .

(ponderosa pine) for wet and dry temperate evergreen, respectively, and Donaldson (Florida slash pine) for subtropical dry evergreen forest. We would like additional evergreen classes for cool nonmontane pines (e.g., white pine) and for hemlock, but flux data are unavailable.

[26] Harvard Forest was the calibration site for deciduous broadleaf forests ($\sim 1.976\%$), which also included IGBP class “deciduous needleleaf forests” (e.g., larch) that do not occur extensively in North America. IGBP mixed forest ($\sim 7.29\%$) was calibrated using Howland (Maine). IGBP closed ($\sim 0.54\%$) and open shrubland ($\sim 8.6\%$) were combined into “shrubland”, and calibrated using Lucky Hills. IGBP woody savannas ($\sim 1.3\%$) and savannas ($\sim 0.14\%$) were combined (“savannas”) and calibrated using Tonzi Ranch. The IGBP class of croplands ($\sim 3.77\%$) was adopted as is and calibrated using data from Mead-S2 (Nebraska) for both irrigated maize and soybeans, planted in rotation.

[27] IGBP “grasslands” ($\sim 3.3\%$), “crop/natural vegetation mosaic” ($\sim 3.9\%$), and “barren or sparsely vegetated lands” ($\sim 1.8\%$) were combined into VPRM “grasslands” and calibrated at the Vaira range site. This class may be affected by significant representation errors when the grassland calibration is applied to crop/natural mosaics, which in the northern tier are often dairy farms interspersed with woodlands. However, there are no data to allow subdivision of these categories. The IGBP “permanent wetlands” ($\sim 0.7\%$) was calibrated at the eastern peatland site in Canada. IGBP classes for water bodies ($\sim 59\%$), urban and built-up ($\sim 0.18\%$), and snow and ice ($\sim 0.27\%$) were combined into our last class, for which vegetation-derived fluxes are assigned as zeros.

[28] Tower data sets provide several versions of NEE: with and without filtering by turbulent intensity (u^*) and with or without gap filling. Some sites also provide GEE and R , separated using various approaches. To avoid possible biases and inconsistencies from filling or separating GEE and R , VPRM parameters were optimized against unfilled tower NEE, with a u^* filter applied to eliminate unrepresentative observations.

[29] The current VPRM is intended to cover vegetation from 11°N to 65°N and 50°W to 145°W , including the continental United States, Mexico, and most of Canada. For large-scale applications the 1-km IGBP vegetation data were

classified into these types and regridded to $10 \times 10 \text{ km}$, or $1/4^\circ \times 1/6^\circ$, retaining information on the fractional coverage for each vegetation type. These data are provided to the public with the VPRM distribution.

3.2. Satellite Data

[30] We analyzed multiyear satellite images from the MODIS sensor aboard the Terra satellite (2000–2003/2004), crossing the equator at 1030 local time. MODIS views the entire surface of the Earth every 1–2 d measuring 36 spectral bands at 250 or 500 m resolution between 0.405 and $14.385 \mu\text{m}$.

[31] We acquired 8-d mean MODIS surface reflectances (MOD09A1) for our calibration and validation sites from the Oak Ridge Distributed Active Archive Center (<http://www.modis.ornl.gov/modis/index.cfm>), which provides time series data for most flux towers in ASCII format. We had to process MODIS subsets directly (Hierarchical Data Format (HDF); <http://landval.gsfc.nasa.gov>) for sites where the MODIS ASCII subsets were unavailable (e.g., Lucky Hill).

[32] The MOD09A1 products give data for nine MODIS pixels covering $1.5 \text{ km} \times 1.5 \text{ km}$, centered on each flux tower. We averaged the 8-d mean surface reflectance data for red (620–670 nm), NIR (841–876 nm), blue (459–479 nm), and SWIR (1628–1652 nm) to calculate EVI and LSWI, then applied a low-order smoothing algorithm (“lowess”, locally weighted least squares) [Cleveland, 1981] to the time series for each to reduce noise associated with imperfect atmospheric corrections in MOD09A1 data.

4. Results

[33] We optimized model parameters (λ , PAR_0 , α , and β ; see Table 2) via nonlinear least squares (Newton-Raphson, tangent linear approximation) and estimated confidence intervals assuming Gaussian errors for both model and tower data. For each calibration site we generated hourly data from the smoothed time series of vegetation indices (EVI and LSWI) and obtained measurements of air temperature and PAR from the tower sites.

[34] Examples of observed and modeled NEE are shown in Figure 2a. The VPRM provides consistent partitioning of

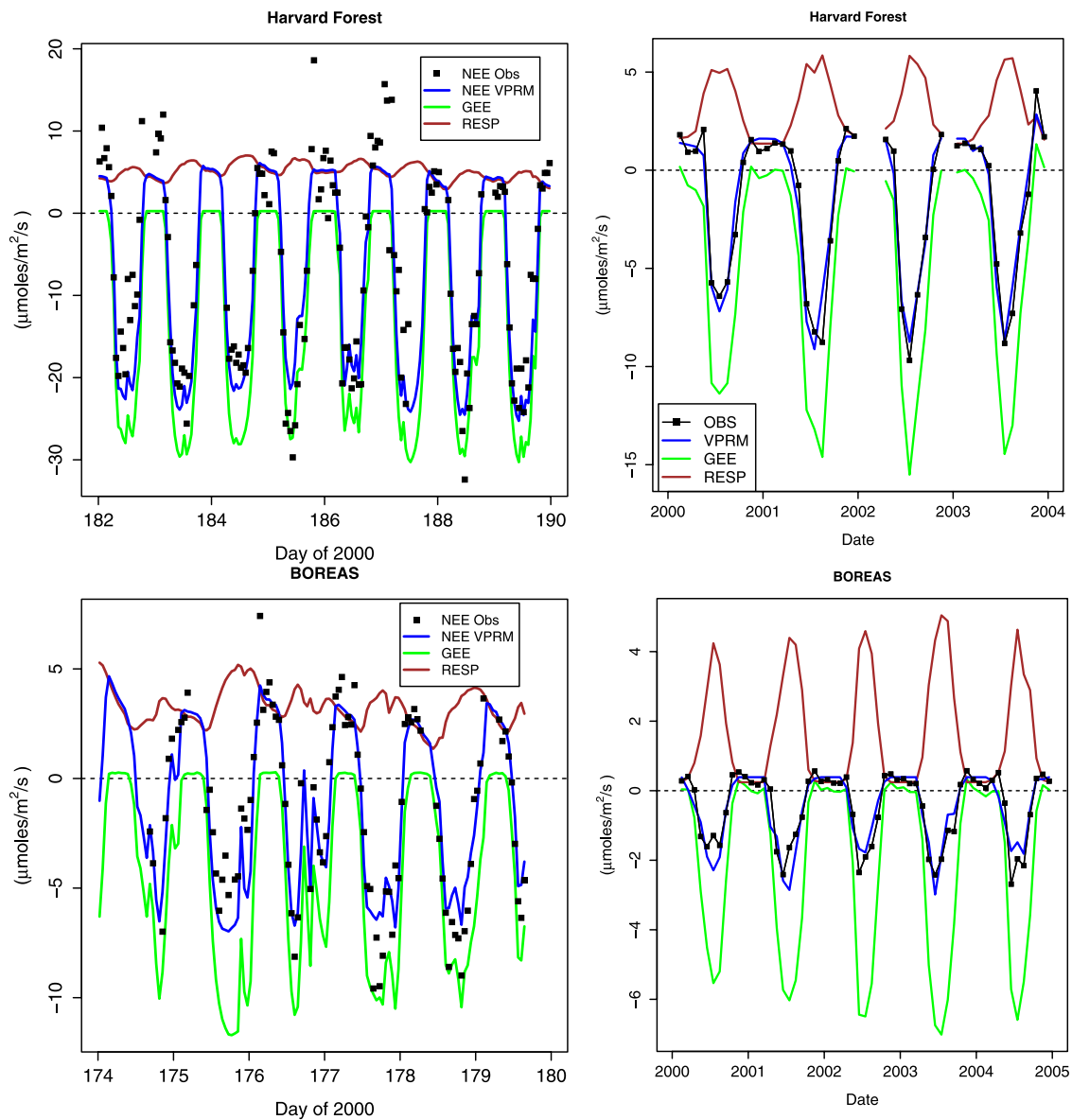


Figure 2a. (left) Examples of hourly output from the VPRM for Harvard Forest (top) and BOREAS/NOBS (bottom). Observations (points) show u^* -filtered hourly data only. (right) Comparison between the observed (solid squares) and VPRM (blue line) monthly mean NEE ($\mu\text{mole m}^{-2} \text{s}^{-1}$) over the 4-year period at these two calibration sites. VPRM provides a consistent separation of the light-dependent part of NEE (“GEE”) from the light-independent part (Respiration) across all sites.

tower NEE data into light-dependent and light-independent parts for all calibration sites, and it thus provides an independent tool for filling missing data (see Figure 2a). (Note that T_{scale} is assumed to define the temperature dependence of photosynthesis.) VPRM has the advantage of incorporating satellite data into the process, and it can be applied to any tower site. It yields consistent, independent estimates of annual net exchange for all sites where the optimization procedure is run.

[35] When driven by high-resolution data sets, the VPRM equations are able to reproduce 1 to 4 years of data with remarkable fidelity, including both diurnal cycles (Figure 2b)

and aggregation to monthly timescales (Figure 3), despite their ultrasimple form. Inputs of accurate solar irradiance and temperatures allow the VPRM to closely track hourly variations; inputs from remote sensing data enable the VPRM to also track the seasonal course of NEE. The model even captures a significant amount of interannual variability, driven by variations in T , PAR, and EVI (Figure 2a, right).

[36] Values of λ for forests and crops range from 0.17 to 0.27 (Table 2), consistent with the expectation that optimum light use efficiency at low light should be $\sim 1:6$ ($\lambda = 0.17$) for a dense vegetation canopy. Values are lower for semiarid grasslands and shrublands, again as expected. Values of r^2

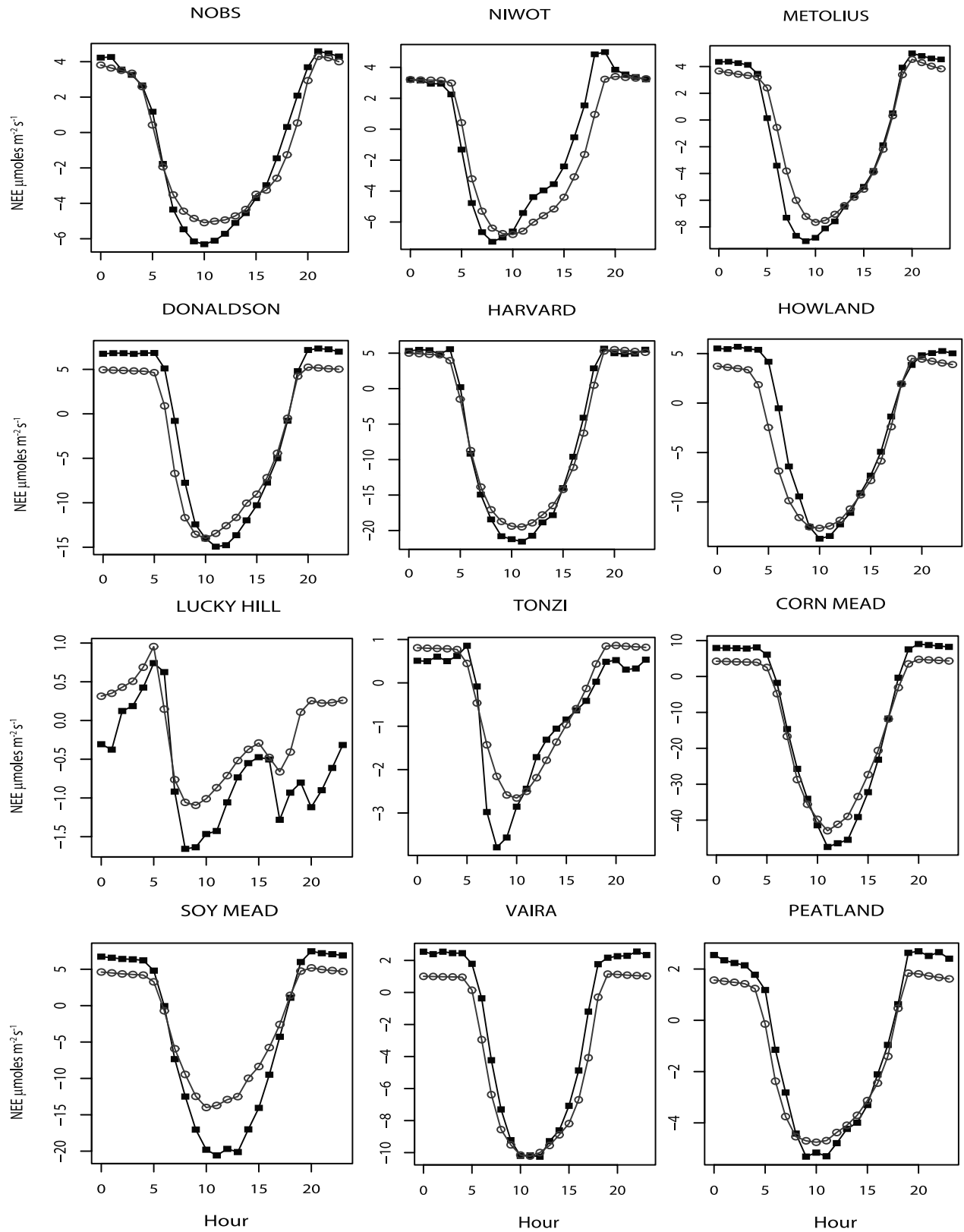


Figure 2b. A comparison between the observed (solid squares) and VPRM (open circles) mean diurnal variation of NEE ($\mu\text{mole m}^{-2} \text{s}^{-1}$) during the peak growing season at calibration sites.

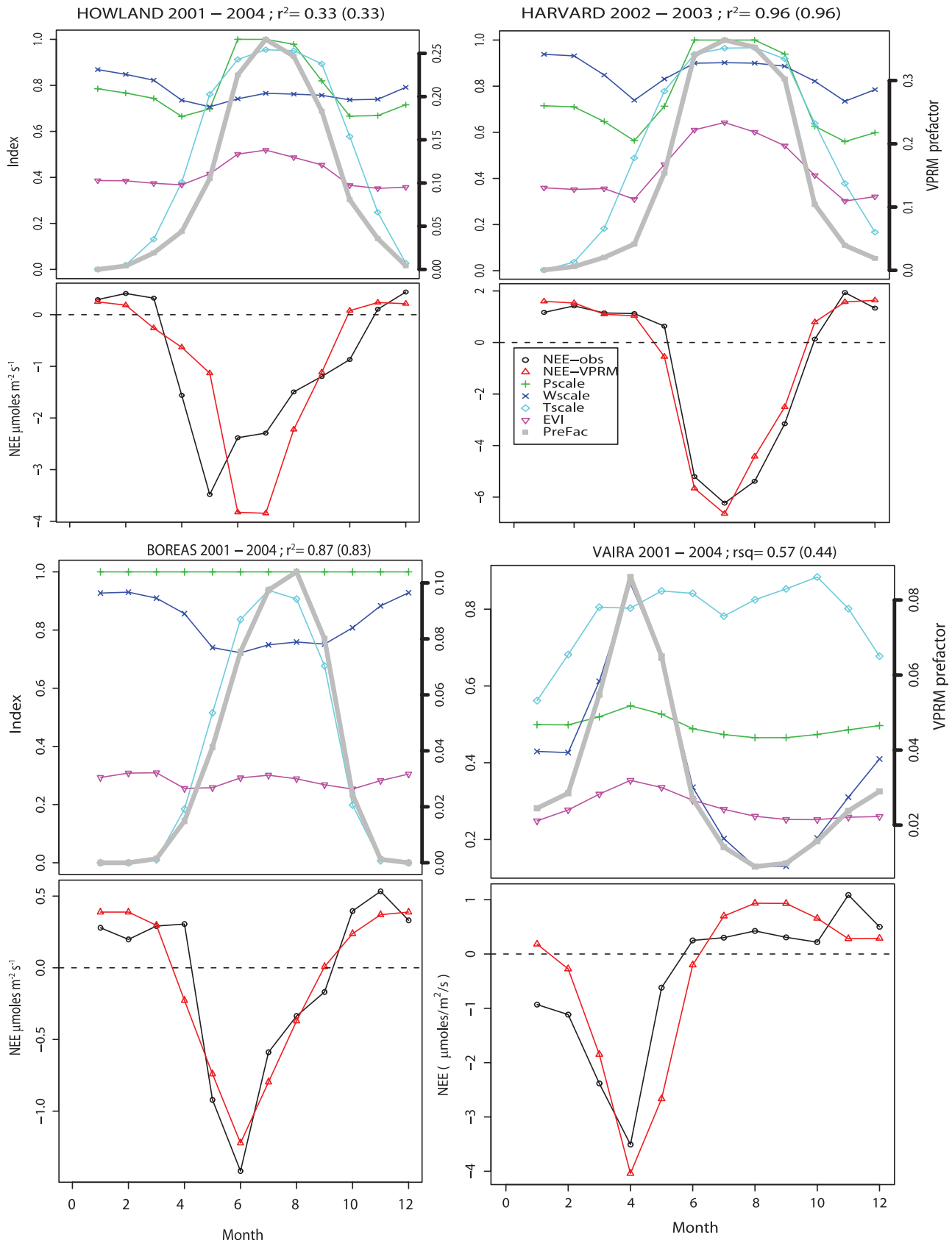


Figure 3

range from 0.6 to 0.9 for calibration sites; correlations are almost as good at many validation sites. Note the high value of PAR_0 (Table 2) for corn, apparently capturing the high LUE [Gower *et al.*, 1999]. PAR_0 values in Table 2 are higher at cropland xeric sites than would be found in conventional analysis of a light curve, where NEE is fit to a hyperbolic function of PAR. Midday summer temperatures often exceed T_{opt} , and hence the VPRM infers high R and low GEE, attributing the decrease in photosynthetic efficiency to excessive heat rather than to light saturation.

[37] Figure 3, top, shows the relationship between the seasonal dynamics of NEE and VPRM photosynthesis factors. As expected, croplands and grasslands respond strongly to phenology (P_{scale}) and the amount of photosynthetically active vegetation (EVI). Likewise, variations in P_{scale} and EVI, as well as light (PAR), strongly modulate the uptake of CO_2 at deciduous and mixed sites (Harvard and Howland), whereas the temperature dependence of photosynthesis (T_{scale}) is the primary factor limiting uptake of CO_2 by well-watered evergreen forests (NOBS, Metolius/Oregon, and Niwot). Intraseasonal trends in the VPRM sometimes were able to capture water stress and changes in EVI.

[38] There are a few surprises. Harvard and Howland forests both include significant evergreen conifers, as typical for “deciduous” and “mixed” forests, and T_{scale} is thus also critically important in limiting uptake at these sites in winter. Donaldson is warm and evergreen, but in winter it is not actually very green at all, and the very low values of EVI limit uptake. The notably poor fit at Donaldson in summer may be particular to the 2001–2002 interval used for calibration; this was the end of a severe, extended drought, and remotely sensed indices might not have captured the associated aftereffects.

[39] Other discrepancies appear to be associated with the inability of remotely sensed data to detect water stress and/or conductance limitations during summer at sites with strong coniferous representation (Donaldson, Metolius, and Howland). Thus the VPRM overpredicts uptake at these sites in middle and late summer, when photosynthesis rates decline steeply but EVI and LSWI change only modestly. At some sites the model does a surprisingly good job in capturing declines in net uptake due to increased respiration in middle and late summer, for example, NOBS/BOREAS [Dunn *et al.*, 2007].

[40] The shrubland site (Lucky Hill) had the worst fit. Carbon dioxide exchanges at this site derive from both organic and soil inorganic pools [Emmerich, 2003]; the latter is beyond the scope of a model like the VPRM.

[41] We carried out VPRM simulations for 11 different validation sites (SOBS, B1850, EOBS, DUKE-PP, INDIANA, DUKE-HW, WCREEK, LCREEK, WLEF, BOND,

and ANLGRASS) using derived model parameters from calibration sites in the same or similar vegetation classes, without any adjustment. SOBS, B1850 and EOBS were classified as old growth evergreen boreal forests, and model parameters were taken from NOBS. DUKE-PP was classified as evergreen dry temperate forest, and model parameters were taken from Metolius. INDIANA and DUKE-HW were classified as deciduous forest and model parameters were taken from Harvard Forest. WCREEK, LCREEK, and WLEF were classified as mixed forest, and model parameters were taken from Howland Forest, although this classification is not completely accurate for WCREEK (a young maple stand) and LCREEK (a major fraction is wetland). Soy and corn at BOND and ANLGRASS were validated using Mead-S2 soy and corn and VAIRA model parameters, respectively. We were not able to test the VPRM independently for other vegetation classes because of lack of tower data.

[42] Most validation simulations were very successful. Figure 4 shows that the diurnal variation of NEE was slightly underestimated at B1850, DUKE-HW, and ANLGRASS and slightly overestimated at BOND-soy and LCREEK. ANLGRASS nighttime respiration was notably underestimated. Figure 5 shows the seasonal variation of NEE at validation sites, and associated VPRM functions, as in Figure 3. Seasonal peaks of NEE were slightly overestimated at DUKE-PP, INDIANA, ANLGRASS, and BOND-SOY.

[43] Overall, when model parameters from calibrated sites were applied to similar ecosystems for validation (Table 3), r^2 values were almost as high as at calibration sites, demonstrating strong predictive ability for sites with similar vegetation. WLEF was an outlier. Several studies have noted [Desai *et al.*, 2008; Wang *et al.*, 2006] the sharp differences between WLEF fluxes versus WCREEK and LCREEK, which are not as similar to each other, or to Howland, as one would like. Mackay *et al.* [2002] compared WLEF stand types to IGBP classes and suggested that four distinct stand types are needed to characterize the region’s evapotranspiration fluxes. Possibly the great tower height affects resolution of surface fluxes, extends the area influencing the tower, or introduces measurement artifacts.

[44] The VPRM provides excellent prediction of monthly NEE for most calibration and validation sites (Figure 6), excluding WLEF. Since the optimization exclusively used hourly data, the excellent agreement between VPRM and observations at the monthly timescale (Table 3), representing aggregation by a factor of ~ 600 in time, indicates successful elimination of bias in the nonlinear optimized functions. Only one calibration site (Donaldson/slash pine) and two of the validation sites (ANL-grassland and Duke Ponderosa pine) fail to scale up in time. These are the sites

Figure 3. (top) Seasonal dynamics of the prefactors T_{scale} , P_{scale} , and W_{scale} in the VPRM equation (equation (11)), driven by satellite and meteorological data. All factors are significant, at various times and places. (bottom) Comparison of the seasonal dynamics between observed (black) and VPRM (red) monthly mean NEE ($\mu\text{mole m}^{-2} \text{s}^{-1}$) at calibration sites, monthly means, averaged over all years. Values in the title bar give the fraction of the total variance of the mean seasonal cycle of NEE captured by the model, $[1 - \text{var}(\text{NEE}_{\text{obs}} - \text{NEE}_{\text{VPRM}})/\text{var}(\text{NEE}_{\text{obs}})]$ (in parenthesis, the same quantity for the time series of individual monthly means). Note that net uptake of CO_2 corresponds to negative values of NEE.

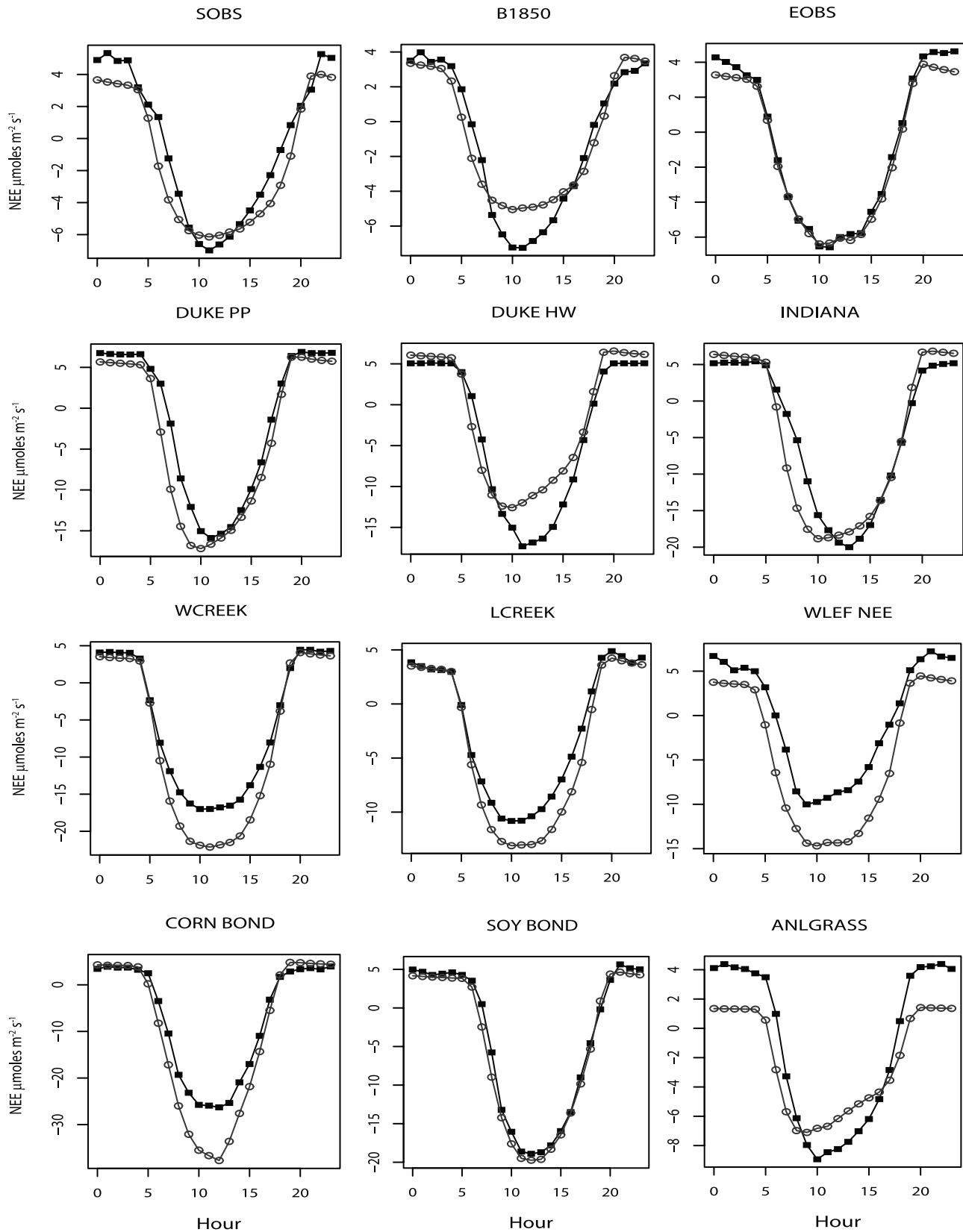


Figure 4. Comparison between the observed (solid squares) and predicted (open circles) diurnal mean NEE ($\mu\text{mole m}^{-2} \text{s}^{-1}$) over the peak photosynthetically active period, as in Figure 2b, but at validation sites without adjustment of parameters.

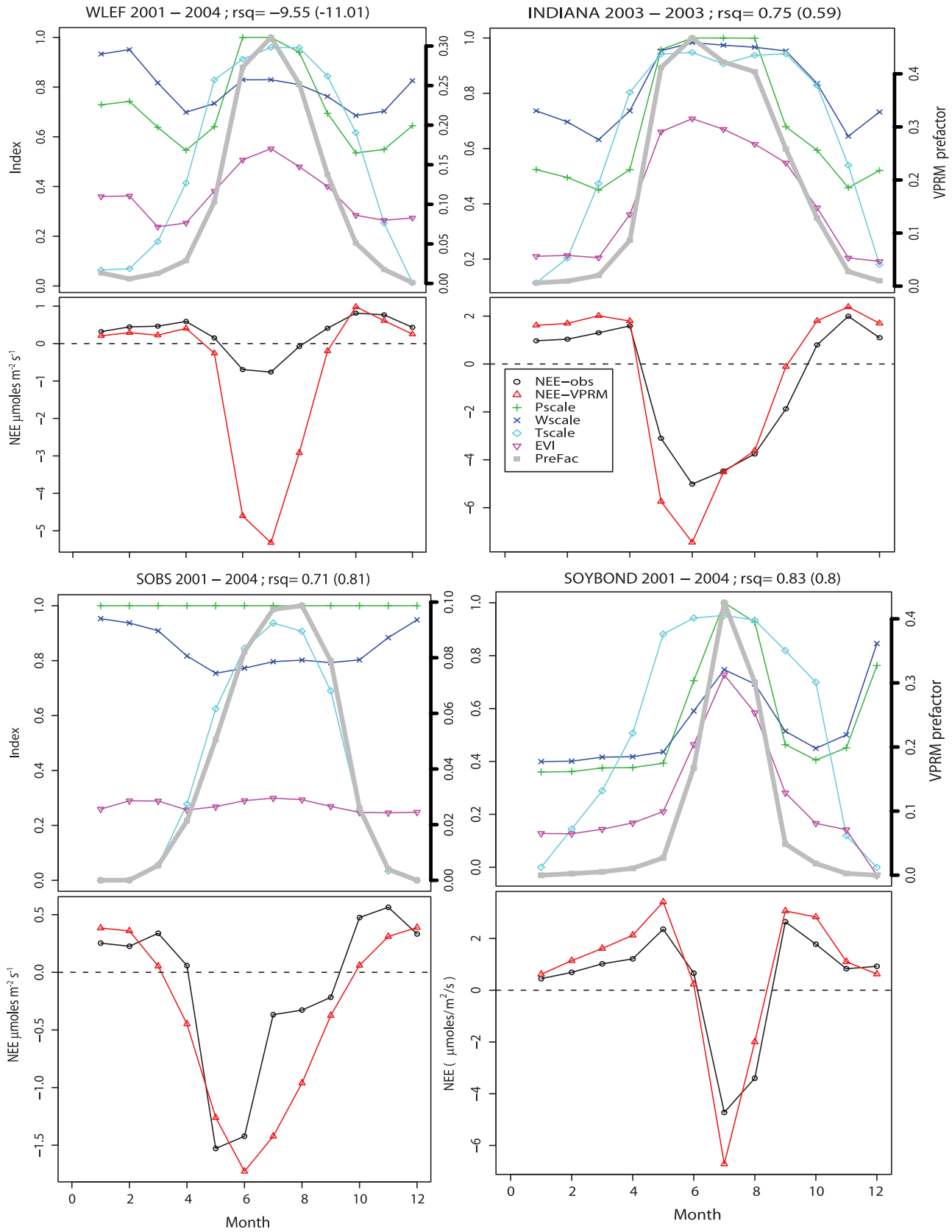


Figure 5. A comparison of the seasonal dynamics of model and observed NEE, as in Figure 3, but at validation sites (no adjustment of VPRM parameters).

Table 3. Correlation Coefficients for Monthly and Hourly NEE and Means for All Seasons and for the Growing Season Hourly Data of Tower Flux and VPRM Calculations at Calibration and Cross-Validation Sites^a

Site	Calibration Site	Years	r ² Monthly	r ² Hourly	Mean NEE-All ($\mu\text{mole m}^{-2}\text{s}^{-1}$)		Growing Seas ($\mu\text{mole m}^{-2}\text{s}^{-1}$)	
					Obs	VPRM	Obs	VPRM
HARVARD	-	4	0.96	0.83	-1.64	-1.70	-7.24	-7.50
HOWLAND	-	4	0.33	0.65	-0.59	-0.59	-1.32	-2.61
NOBS	-	4	0.83	0.72	-0.54	-0.59	-1.75	-1.96
NIWOT	-	4	0.25	0.56	-0.19	-0.19	-0.85	-1.13
METOLIUS	-	3	0.55	0.63	-0.99	-0.99	-1.66	-1.31
SOY_MEADS2	-	1	0.61	0.66	0.08	0.05	-2.32	-2.05
CORN_MEADS2	-	1	0.94	0.83	-1.54	-1.58	-8.13	-9.42
TONZI	-	3	0.57	0.43	-0.59	-0.59	-1.22	-0.81
VAIRA	-	3	0.44	0.55	-0.42	-0.43	-1.33	-2.43
DONALDSON	-	2	-1.04	0.82	-1.49	-1.52	-1.15	-2.12
LUCKY-HILLS	-	4	0.36	0.46	0.02	0.01	0.31	0.74
PEATLAND	-	1	0.50	0.71	-0.04	-0.04	-0.77	-1.06
SOBS	NOBS	5	0.81	0.69	-0.88	-1.23	-2.04	-2.83
EOBS	NOBS	1	0.88	0.74	-0.51	-0.29	-1.91	-1.70
B1850	NOBS	4	0.84	0.62	-0.66	-0.57	-1.97	-1.69
DUKE_PP	METOLIUS	4	-0.43	0.58	-1.01	-2.63	-1.66	-4.89
DUKE_HW	HARVARD	4	0.64	0.58	-1.00	0.47	-3.59	-1.80
INDIANA	HARVARD	4	0.59	0.65	-0.70	-0.40	-4.35	-4.94
WCREEK	HOWLAND	5	0.77	0.77	-0.87	-1.78	-5.36	-7.95
LCREEK	HOWLAND	4	0.53	0.66	-0.27	-0.18	-2.12	-2.68
WLEF	HOWLAND	2	-11.0	0.46	0.26	-0.37	-0.52	-3.94
SOY_BOND	SOY_MEAD	1	0.80	0.72	0.31	0.85	-2.62	-3.02
CORN_BOND	CORN_MEAD	1	0.76	0.63	-1.27	-0.53	-7.02	-9.03
ANLGRASS	VAIRA	2	-0.40	0.57	-0.34	-0.80	-0.52	-1.32

^aOnly intersection data (available in both observation and model columns) were used. Growing season hourly data: April to June for VAIRA and ANLGRASS; June to August for all other sites. Correlation coefficients: r².

are likely affected by water stress, which we already noted may not be accurately captured in the VPRM.

[45] The VPRM validations did not capture the seasonal cycle as well at boreal evergreen forests (SOBS, B1850, and EOBS; see Table 3) as at other sites. These biomes exhibit an especially strong seasonal cycle of ecosystem respiration,

controlled by subsurface processes such as slow thawing and draining of snowmelt-saturated soils [Dunn *et al.*, 2007] that are not remotely sensible, as well as prior site history. Thus the VPRM cannot distinguish the late summer trends at these sites on the basis of the fit to the NOBS data.

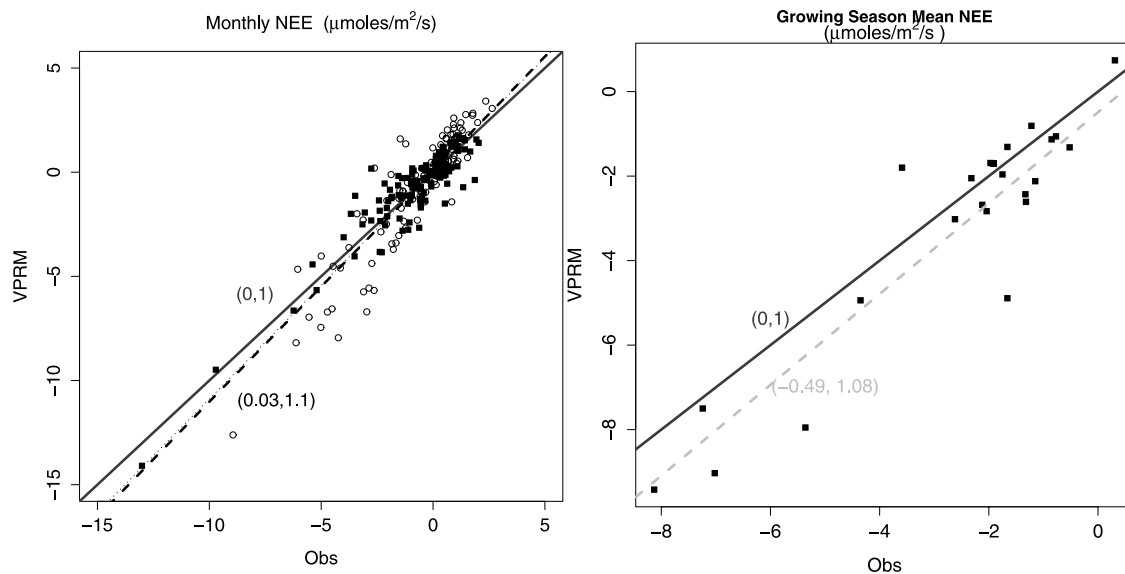


Figure 6. (left) Observed and predicted monthly mean NEE ($\mu\text{mole m}^{-2}\text{s}^{-1}$) for calibration sites (solid symbols) and validation sites (open symbols) excluding WLEF. Regression line for all sites (dotted line) is very similar to the regression for validation sites only (dashed line). (right) Mean NEE by site (except WLEF) for the growing season. Line labeled (0,1) has zero intercept and slope = 1 (“1:1 line”). Regression lines are labeled similarly.

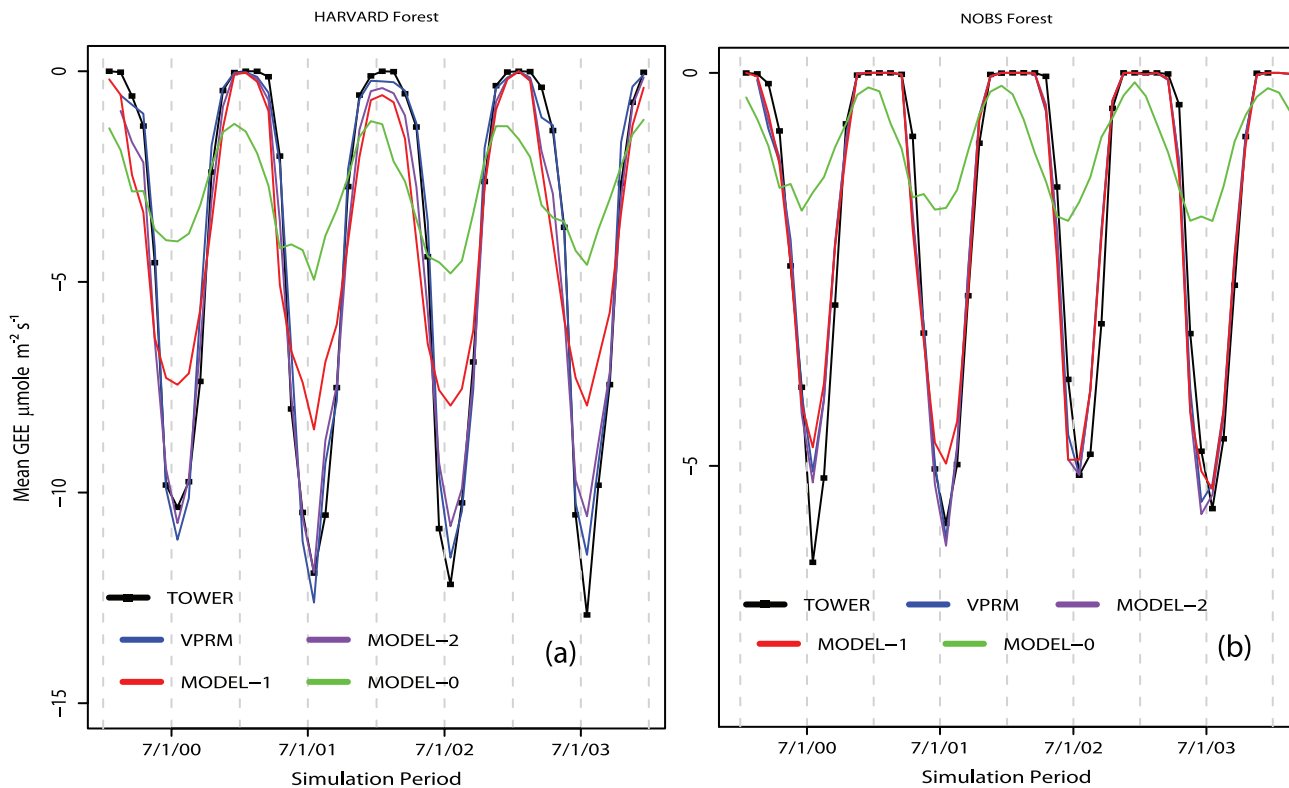


Figure 7. A comparison between GEE ($\mu\text{mole m}^{-2} \text{s}^{-1}$) obtained by fitting VPRM, MODEL-2, MODEL-1, and MODEL-0 to tower data from 2000 to 2003 at Harvard Forest (a) and NOBS/BOREAS (b). VPRM incorporates EVI, P_{scale} , and W_{scale} (driven by satellite data), plus T_{scale} driven by meteorological data. MODEL-2 drops LSWI factors (P_{scale} and W_{scale}), MODEL-1 drops all satellite

[46] We quantified the role of satellite vegetation indices and of the temperature function for photosynthesis (T_{scale}) using a series of reduced models. Each was optimized independently using NEE data for Harvard and NOBS, then compared to the VPRM:

$$NEE_{\text{model-2}} = -\lambda' \times T_{\text{scale}} \times \frac{1}{(1 + PAR/PAR'_0)} \times EVI \times PAR + \alpha' \times T + \beta' \quad (13)$$

$$NEE_{\text{model-1}} = -\lambda'' \times T_{\text{scale}} \times \frac{1}{(1 + PAR/PAR''_0)} \times PAR + \alpha'' \times T + \beta'' \quad (14)$$

$$NEE_{\text{model-0}} = -\lambda''' \times \frac{1}{(1 + PAR/PAR'''_0)} \times PAR + \alpha''' \times T + \beta''' \quad (15)$$

Model-2 deletes the water and phenology scaling factors using LSWI, Model-1 deletes all satellite information (LSWI and EVI), and Model-0 deletes these and also drops T_{scale} .

[47] Figure 7 compares GEE from the VPRM to GEE from these reduced models, and to GEE partitioned from eddy flux data. At Harvard the shaping of the uptake curve by P_{scale} plays a role, and inter- and intraseasonal changes of EVI are very important (Figure 7a). The role of T_{scale} is surprisingly significant, as noted above, and omitting T_{scale} ruins the seasonal fit at Harvard.

[48] Data inputs from LSWI and EVI are much less important for representing fluxes from boreal evergreens (Figure 7b), as expected. However, interannual variations of EVI appear significant in capturing interannual variations of GEE. At this site also, no good fit can be obtained unless T_{scale} is included to limit photosynthesis in cold weather.

5. Discussion

[49] This paper develops and validates the VPRM, a satellite-based vegetation photosynthesis and respiration model, intended to provide NEE over North America with fine temporal and spatial resolution. The model has very simple structure and few adjustable parameters. It was tested using observations from all across the AmeriFlux and Fluxnet-Canada networks. When combined with maps of vegetation type, meteorological data for temperature, and satellite-derived shortwave radiation, it provides an excellent a priori representation of surface CO_2 fluxes, with

hourly time resolution and spatial resolution equal to that of the vegetation data (1 km for the IGBP).

[50] There are many process-based biogeochemical models (e.g., SiB2 or Biome-BGC) that simulate the storage and fluxes of water, carbon, and nitrogen by vegetation, litter, and soil. They can provide estimates of net primary production (NPP) or gross primary production (GPP), and in some cases, NEE, with hourly resolution. However, these models require complex parameter specification. For example, 47 parameters were spatially interpolated for regional simulations of SiB2 [Wang *et al.*, 2007a]. In many cases, model parameters need frequent recalibration within short time periods, and the models may incur significant computational effort.

[51] The data-driven approach of the VPRM is capable of reproducing spatial and temporal variations of NEE using simple equations plus a compact database derived from MODIS. There are only four parameters per vegetation type that persist for the whole annual cycle, with spatial and temporal variations rendered by high-resolution meteorological and remote sensing data.

[52] Statistical uncertainties in the VPRM are given in Tables 2 and 3. Important additional systematic errors arise in part from the model structure. The lack of a soil moisture component and inability to remotely sense water stress are discussed above. Errors also arise because of limited resolution in the vegetation classification. Calibration and validation sites do not have identical vegetation assemblages, and the landscape includes assemblages not represented at all in present networks (e.g., northern white pine forests and loblolly pine plantations). Differences in vegetation functional responses are associated with climate, soil properties and soil moisture, canopy structure, necromass, and tree ages and distribution, none of which can currently be resolved using tower site data. Related errors arise from misclassification by the IGBP (e.g., at LCREEK).

[53] Noise in MODIS data also introduces significant errors in EVI and LSWI, and the noisy time series of MODIS data leads to errors in phenology. Notably large errors in model NEE accrue because of deficiencies in the driver data (sunlight and temperature), affecting CO₂ flux predictions from all surface flux models. Detailed studies of errors in driver data will be described in a subsequent paper.

6. Conclusions

[54] The VPRM assimilates large amounts of data from remote sensing, meteorology, and flux towers and compresses the acquired knowledge into just four parameters in each vegetation class. Vegetation indices (EVI and LSWI) from the MODIS sensor, representation of the temperature dependence of photosynthesis, and accurate driver data are all that is required to describe the hourly and seasonal dynamics of NEE across the landscape. When coupled to accurate data sets for these factors, the VPRM partitions NEE into GEE (light-dependent) and *R* (light-independent) without complex algorithms or submodels, and with a minimal resort to arbitrary assumptions. The four parameters of the VPRM drive a model with very simple structure

that demonstrates strong predictive ability for NEE from hourly to monthly timescales.

[55] The selected calibration and validation sites provide a minimal representation of the vegetation of North America. At present, over 200 eddy flux tower sites make up a global FLUXNET network (<http://www.daac.ornl.gov/FLUXNET>). Data for CO₂, H₂O, and energy flux for numerous ecosystem types have been accumulated; but availability of quality-assured data has not kept pace. Once multiyear data from more eddy flux tower sites are available, the VPRM can be refined and extended across a wider range of ecosystem and climate and soil conditions, and to other continents. Enhanced vegetation classification, including stand ages, would provide the basis for further improvements while conserving the simple structure of the VPRM.

[56] The VPRM can be applied at the scale of North American, providing a detailed representation of the spatio-temporal variation of CO₂ fluxes across the landscape, with a low-dimensional parameter space for optimization in an inverse model framework. The calibrated model coefficients (λ , PAR₀, α , and β) represent a priori parameter estimates. We envision the principal application of the VPRM to be reoptimization of the parameters at local, regional, or continental scales in top down analyses of carbon fluxes. The model and underlying databases are publicly available at (<http://www-as.harvard.edu/data/>).

[57] **Acknowledgments.** We would like to thank the flux site investigators for providing their data through AmeriFlux and Fluxnet-Canada programs. This study was supported at Harvard University by a grant from the National Science Foundation Bio-complexity in the Environment Program (ATM-0221850) and by grants from the U.S. Department of Energy in the Terrestrial Carbon Program, grant DE-FG02-98ER62695, and the Northeast Regional Center (NERC) of the National Institute for Global Environmental Change (NIGEC) under cooperative agreement DE-FCO2-03ER63613; also by NASA grants NAG5-11154 and NNG05GA76G from the Terrestrial Ecological Program. We also thank William E. Emmerich for providing Lucky Hills flux data from the USDA-ARS Agriflux Carbon project. The research at Duke Forest was supported by the Office of Science (BER), U.S. Department of Energy, grant DE-FG02-00ER63015 (Hardwood Forest), and through its Southeast Regional Center (SERC) of the NIGEC under cooperative agreement DE-FCO2-03ER63613 (Pine Plantation). The research at the Metolius ponderosa pine site was supported by the Office of Science (BER), U.S. Department of Energy, grant DE-FG0203ER63653.

References

- Aber, J. D., and C. A. Federer (1992), A generalized, lumped-parameter model of photosynthesis, evapotranspiration, and net primary production in temperate and boreal forest ecosystems, *Oecologia*, 92, 463–474.
- Baker, D. F., S. C. Doney, and S. D. Schimel (2006), Variational data assimilation for atmospheric CO₂, *Tellus, Ser. B*, 58, 359–365.
- Bakwin, P. S., P. P. Tans, D. F. Hurst, and C. Zhao (1998), Measurements of carbon dioxide on very tall towers: Results of the NOAA/CMDL program, *Tellus, Ser. B*, 50, 410–415.
- Baldocchi, D. D., et al. (2001), FLUXNET: A new tool to study the temporal and spatial variability of ecosystem-scale carbon dioxide, water vapor, and energy flux densities, *Bull. Am. Meteorol. Soc.*, 82, 2415–2435.
- Baldocchi, D. D., L. Xu, and N. Kiang (2004), How plant functional-type, weather, seasonal drought, and soil physical properties alter water and energy fluxes of an oak-grass savanna and an annual grassland, *Agric. For. Meteorol.*, 123, 13–39.
- Belward, A. S., J. E. Estes, and K. D. Kline (1999), The IGBP-DIS global 1-km land-cover data set DISCover: A project overview, *Photogramm. Eng. Remote Sens.*, 65(9), 1013–1020.
- Bergeron, O., H. A. Margolis, A. Black, C. Coursolle, A. L. Dunn, A. G. Barr, and S. C. Wofsy (2007), Comparison of carbon dioxide fluxes over

- three boreal black spruce forests in Canada, *Global Change Biol.*, *13*, 89–117.
- Boles, S., X. Xiao, J. Liu, Q. Zhang, S. Munkhtuya, and S. Chen (2004), Land cover characterization of temperate East Asia using multi-temporal VEGETATION sensor data, *Remote Sens. Environ.*, *90*, 477–489.
- Clark, K. L., H. L. Gholz, J. B. Moncrieff, F. Cropley, and H. W. Loescher (1999), Environmental controls over net exchanges of carbon dioxide from contrasting Florida ecosystems, *Ecol. Appl.*, *9*(3), 936–948.
- Clark, K. L., H. L. Gholz, and M. S. Castro (2004), Carbon dynamics along a chronosequence of slash pine plantations in north Florida, *Ecol. Appl.*, *14*(4), 1154–1171.
- Cleveland, W. S. (1981), LOWESS: A program for smoothing scatterplots by robust locally weighted regression, *Am. Stat.*, *35*, 54–54J.
- Cook, B. D., et al. (2004), Carbon exchange and venting anomalies in an upland deciduous forest in northern Wisconsin, USA, *Agric. For. Meteorol.*, *126*, 271–295.
- Coops, N. C., R. H. Waring, and B. E. Law (2005), Assessing the past and future distribution and productivity of ponderosa pine in the Pacific Northwest using a process model, 3-PG, *Ecol. Modell.*, *183*(1), 107–124.
- Coulter, R. L., M. S. Pekour, D. R. Cook, G. E. Klazura, T. J. Martin, and J. D. Lucas (2006), Surface energy fluxes and carbon dioxide fluxes above different vegetation types within ABLE, *Agric. For. Meteorol.*, *136*, 147–158.
- Cunningham, S. C. (2005), Photosynthetic responses to vapor pressure deficit in temperate and tropical evergreen rainforest trees of Australia, *Oecologia*, *142*(4), 521–528.
- Davidson, E. A., K. Savage, L. V. Verchot, and R. Navarro (2002a), Minimizing artifacts and biases in chamber-based measurements of soil respiration, *Agric. For. Meteorol.*, *113*, 21–37.
- Davidson, E. A., et al. (2002b), Belowground carbon allocation in forests estimated from litterfall and IRGA-based soil respiration measurements, *Agric. For. Meteorol.*, *113*, 39–51.
- Davis, K. J., P. S. Bakwin, C. X. Yi, B. W. Berger, C. L. Zhao, R. M. Teclaw, and J. G. Isebrands (2003), The annual cycles of CO₂ and H₂O exchange over a northern mixed forest as observed from a very tall tower, *Global Change Biol.*, *9*, 1278–1293.
- Denning, A. S., I. Y. Fung, and D. Randall (1995), Latitudinal gradient of atmospheric CO₂ due to seasonal exchange with land biota, *Nature*, *376*, 240–243.
- Desai, A., P. V. Bolstad, B. D. Cook, K. J. Davis, and E. V. Carey (2005), Comparing net ecosystem exchange of carbon dioxide between an old-growth and mature forest in the upper Midwest, USA, *Agric. For. Meteorol.*, *128*(1–2), 33–55.
- Desai, A., et al. (2008), Influence of vegetation and seasonal forcing on carbon dioxide fluxes across the Upper Midwest, USA: Implications for regional scaling, *Agric. For. Meteorol.*, *148*, 288–308.
- Diak, G. R., J. R. Mecikalski, M. C. Anderson, J. M. Norman, W. P. Kustas, R. D. Torn, and R. L. DeWolf (2004), Estimating land surface energy budgets from space—Review and current efforts at the University of Wisconsin-Madison and USDA-ARS, *Bull. Am. Meteorol. Soc.*, *85*, 65–78.
- Dunn, A. L., C. C. Barford, S. C. Wofsy, M. L. Goulden, and B. C. Daube (2007), A long-term record of carbon exchange in a boreal black spruce forest: Means, responses to inter-annual variability, and decadal trends, *Global Change Biol.*, *13*, 577–590.
- Emmerich, W. E. (2003), Carbon dioxide fluxes in a semiarid environment with high carbonate soils, *Agric. For. Meteorol.*, *116*, 91–102.
- Field, C. B., T. J. Randerson, and C. M. Malmstrom (1995), Global net primary production—Combining ecology and remote-sensing, *Remote Sens. Environ.*, *51*, 74–88.
- Friedl, M. A., X. Zhang, and E. Tsvetinskaya (2003), Observing and deriving land cover properties and dynamics for use in weather and climate models, Annu. Meet. Am. Meteorol. Soc., paper J8.1, Long Beach, Calif., 9–13 February.
- Fung, I. (1993), Models of oceanic and terrestrial sinks of anthropogenic CO₂: A review of the contemporary carbon cycle, in *The Biogeochemistry of Global Change: Radiative Trace Gases*, edited by R. S. Oremland, pp. 166–189, CRC Press, Boca Raton, Fla.
- Fung, I. Y., C. J. Tucker, and K. C. Prentice (1987), Application of advanced very high resolution radiometer to study atmosphere-biosphere exchange of CO₂, *J. Geophys. Res.*, *92*, 2999–3015.
- Gerbig, C., J. C. Lin, S. C. Wofsy, B. C. Daube, A. E. Andrews, B. B. Stephens, P. S. Bakwin, and C. A. Grainger (2003a), Towards constraining regional scale fluxes of CO₂ with atmospheric observations over a continent: 1. Observed spatial variability from airborne platforms, *J. Geophys. Res.*, *108*(D24), 4756, doi:10.1029/2002JD003018.
- Gerbig, C., J. C. Lin, S. C. Wofsy, B. C. Daube, A. E. Andrews, B. B. Stephens, P. S. Bakwin, and C. A. Grainger (2003b), Towards constrain- ing regional scale fluxes of CO₂ with atmospheric observations over a continent: 2. Analysis of COBRA data using a receptor-oriented framework, *J. Geophys. Res.*, *108*(D24), 4757, doi:10.1029/2003JD003770.
- Gerbig, C., J. C. Lin, J. W. Munger, and S. C. Wofsy (2005), What can tracer observations in the continental boundary layer tell us about fluxes?, *Atmos. Chem. Phys. Disc.*, *5*, 9249–9290.
- Goetz, S. J., and S. D. Prince (1999), Modeling terrestrial carbon exchange and storage: The evidence for and implications of functional convergence in light use efficiency, *Adv. Ecol. Res.*, *28*, 57–92.
- Goulden, M. L., J. W. Munger, S. M. Fan, B. C. Daube, and S. C. Wofsy (1996), Measurements of carbon storage by long-term eddy correlation: Methods and a critical evaluation of accuracy, *Global Change Biol.*, *2*, 169–182.
- Goulden, M. L., et al. (1998), Sensitivity of boreal forest carbon balance to soil thaw, *Science*, *279*, 214–217.
- Goulden, M. L., G. C. Winston, A. M. S. McMillan, M. E. Litvak, E. L. Read, A. V. Rocha, and J. R. Elliot (2006), An eddy covariance mesonet to measure the effect of forest age on land-atmosphere exchange, *Global Change Biol.*, *12*, 2146–2162.
- Gower, S. T., C. J. Kucharik, and J. M. Norman (1999), Direct and indirect estimation of leaf area index, fAPAR and net primary production of terrestrial ecosystems, *Remote Sens. Environ.*, *70*, 29–51.
- Grace, J., and M. Rayment (2000), Respiration in the balance, *Nature*, *404*, 819–820.
- Griffis, T. J., T. A. Black, K. Morgenstern, A. G. Barr, Z. Nestic, G. B. Drewitt, D. Gaumont-Guay, and J. H. McCaughey (2003), Ecophysiological controls on the carbon balances of three southern boreal forests, *Agric. For. Meteorol.*, *117*, 53–71.
- Hollinger, D. Y., S. M. Goltz, E. A. Davidson, J. T. Lee, K. Tu, and H. T. Valentine (1999), Seasonal patterns and environmental control of carbon dioxide and water vapor exchange in an ecotonal boreal forest, *Global Change Biol.*, *5*, 891–902.
- Hollinger, S. E., C. J. Bernacchi, and T. P. Meyers (2005), Carbon budget of mature no-till ecosystem in North Central Region of the United States, *Agric. For. Meteorol.*, *130*, 59–69.
- Huete, A. R., H. O. Liu, K. Batchily, and W. V. Leeuwen (1997), A comparison of vegetation indices global set of TM images for EOS-MODIS, *Remote Sens. Environ.*, *59*(3), 440–451.
- Huete, A., K. Didan, T. Miura, E. P. Rodriguez, X. Gao, and L. G. Ferreira (2002), Overview of the radiometric and biophysical performance of the MODIS vegetation indices, *Remote Sens. Environ.*, *83*, 195–213.
- Katul, G. G., R. Leuning, J. Kim, O. T. Denmead, A. Miyata, and Y. Harazono (2001), Estimating CO₂ source/sink distributions within a rice canopy using higher-order closure model, *Boundary Layer Meteorol.*, *98*, 103–125.
- Lafleur, P. M., N. T. Roulet, and S. W. Admiraal (2001), The annual cycle of CO₂ exchange from a bog peatland, *J. Geophys. Res.*, *106*, 3071–3082.
- Lafleur, P. M., N. T. Roulet, J. L. Bubier, T. R. Moore, and S. Frothingham (2003), Interannual variability in the peatland-atmosphere carbon dioxide exchange at an ombrotrophic bog, *Global Biogeochem. Cycles*, *17*(2), 1036, doi:10.1029/2002GB001983.
- Lafont, S., L. Kergoat, G. Dedieu, A. Chevillard, E. Kjellström, U. Karstens, and O. Kolle (2002), Spatial and temporal variability of land CO₂ fluxes estimated with remote sensing and analysis data over western Eurasia, *Tellus, Ser. B*, *54*, 820–833.
- Lin, J. C., C. Gerbig, S. C. Wofsy, A. E. Andrews, B. C. Daube, C. A. Grainger, B. B. Stephens, P. S. Bakwin, and D. Y. Hollinger (2004), Measuring fluxes of trace gases at regional scales by Lagrangian observations: Application to the CO₂ Budget and Rectification Airborne (COBRA) study, *J. Geophys. Res.*, *109*, D15304, doi:10.1029/2004JD004754.
- MacKay, D. S., D. E. Ahl, B. E. Ewers, S. T. Gower, S. N. Burrows, S. Samanta, and K. J. Davis (2002), Effects of aggregated classifications of forest composition on estimates of evapotranspiration in a northern Wisconsin forest, *Global Change Biol.*, *8*, 1253–1265.
- Makela, A., P. Kolari, J. Karimaki, E. Nikinmaa, M. Peramaki, and P. Hari (2006), Modeling five years of weather-driven variation of GPP in a boreal forest, *Agric. For. Meteorol.*, *139*, 382–398.
- Meyers, T. P., and S. E. Hollinger (2004), An assessment of storage terms in the surface energy balance of maize and soybean, *Agric. For. Meteorol.*, *125*, 105–115.
- Mitchell, K. E., et al. (2004), The multi-institution North American Land Data Assimilation System (NLDAS): Utilizing multiple GCIIP products and partners in a continental distributed hydrological modeling system, *J. Geophys. Res.*, *109*, D07S90, doi:10.1029/2003JD003823.
- Monserud, R. A., and R. Leemans (1992), Comparing global vegetation maps with the kappa-statistic, *Ecol. Modell.*, *62*(4), 275–293.
- Monson, R. K., A. A. Turnipseed, J. P. Sparks, L. E. Scott-Denton, K. Sparks, and T. E. Huxman (2002), Carbon sequestration in a high-elevation, subalpine forest, *Global Change Biol.*, *8*, 459–478.

- Monteith, J. L. (1972), Solar radiation and productivity in tropical ecosystem, *J. Appl. Ecol.*, *9*, 747–766.
- Oren, R., C.-I. Hsieh, P. Stoy, J. Albertson, H. R. McCarthy, P. Harrell, and G. G. Katul (2006), Estimating the uncertainty in annual net ecosystem carbon exchange: Spatial variation in turbulent fluxes and sampling errors in eddy-covariance measurements, *Global Change Biol.*, *12*, 883–896.
- Pathmathevan, M., T. Koike, X. Li, and H. Fujii (2003), A simplified land data assimilation scheme and its application to soil moisture experiments in 2002 (SMEX02), *Water Resour. Res.*, *39*(12), 1341, doi:10.1029/2003WR002124.
- Piovesan, G., and J. M. Adams (2000), Carbon balance gradient in European forests: Interpreting EUROFLUX, *J. Vegetation Sci.*, *11*, 923–926.
- Potter, C. S., J. T. Randerson, C. B. Field, P. A. Matson, P. M. Vitousek, H. A. Mooney, and S. A. Klooster (1993), Terrestrial ecosystem production: A process model based on global satellite and surface data, *Global Biogeochem. Cycles*, *7*, 811–841.
- Potter, C. S., S. A. Klooster, and V. Brooks (1999), Inter-annual variability in terrestrial net primary production: Exploration of trends and controls on regional to global scales, *Ecosystems*, *2*, 36–48.
- Powell, T. L., R. Bracho, J. H. Li, S. Dore, C. R. Hinkle, and B. G. Drake (2006), Environmental controls over net ecosystem carbon exchange of scrub oak in central Florida, *Agric. For. Meteorol.*, *141*(1), 19–34.
- Prince, S. D., and S. N. Goward (1995), Global primary production: A remote sensing approach, *J. Biogeogr.*, *22*, 815–835.
- Raich, J. W., E. B. Rastetter, J. M. Melillo, D. W. Kicklighter, P. A. Steudler, B. J. Peterson, A. L. Grace, B. Moore, and C. J. Vorosmarty (1991), Potential net primary productivity in South America: Application of a global-model, *Ecol. Appl.*, *1*, 399–429.
- Ruimy, A., P. G. Jarvis, D. D. Baldocchi, and B. Saugier (1995), CO₂ fluxes over plant canopies and solar radiation: A review, *Adv. Ecol. Res.*, *26*, 1–68.
- Running, S. W., P. E. Thornton, R. Nemani, and J. M. Glassy (2000), Global terrestrial gross and net primary productivity from the Earth Observing System, in *Methods in Ecosystem Science*, edited by O. E. Sala et al., pp. 44–57, Springer, New York.
- Schmid, H. P., C. S. B. Grimmond, F. Cropley, B. Offerle, and H.-B. Su (2000), Measurements of CO₂ and energy fluxes over a mixed hardwood forest in the midwestern United States, *Agric. For. Meteorol.*, *103*, 355–373.
- Sellers, P. J., D. A. Randall, G. J. Collatz, J. A. Berry, C. B. Field, D. A. Dazlich, C. Zhang, G. D. Collelo, and L. Bounoua (1996), A revised land surface parameterization (SiB2) for atmospheric GCMs. Part I: Model formulation., *J. Clim.*, *9*, 676–705.
- Song, J., and M. L. Wesely (2003), Evaluation of modeled surface fluxes with aircraft observations, *Agric. For. Meteorol.*, *117*, 159–171.
- Song, J., M. L. Wesely, D. J. Holdridge, and D. R. Cook (2006), Estimating the long-term hydrological budget over heterogeneous surfaces, *J. Hydrometeorol.*, *7*(1), 203–214.
- Stoy, P. C., G. G. Katul, M. B. S. Siqueira, J.-Y. Juang, H. R. McCarthy, H.-S. Kim, A. C. Oishi, and R. Oren (2005), Variability in net ecosystem exchange from hourly to inter-annual time scales at adjacent pine and hardwood forests: A wavelet analysis, *Tree Physiol.*, *25*, 887–902.
- Su, H.-B., H. P. Schmid, C. S. B. Grimmond, C. S. Vogel, and A. J. Oliphant (2004), Spectral characterizes and correction of long-term eddy-covariance measurements over two mixed hardwood forests in non-flat terrain, *Boundary Layer Meteorol.*, *110*, 213–253.
- Tans, P. P. (1980), On calculating the transfer of c-13 in reservoir models of the carbon-cycle, *Tellus*, *32*(5), 464–469.
- Tans, P. P., J. A. Berry, and R. F. Keeling (1993), Oceanic ¹³C/¹²C observations, a new window on CO₂ uptake by the oceans, *Global Biogeochem. Cycles*, *7*, 353–368.
- Tucker, C. J. (1979), Red and photographic infrared linear combination for monitoring vegetation, *Remote Sens. Environ.*, *8*, 127–150.
- Turner, D. P., S. Urbanski, D. Bremer, S. C. Wofsy, T. Meyers, S. T. Gower, and M. Gregory (2003), A cross-biome comparison of daily light use efficiency for gross primary production, *Global Change Biol.*, *9*, 383–395.
- Verma, S. B., et al. (2005), Annual carbon dioxide exchange in irrigated and rainfed maize-based agroecosystems, *Agric. For. Meteorol.*, *131*, 77–96.
- Wang, W., K. J. Davis, B. D. Cook, M. P. Butler, and D. M. Ricciuto (2006), Decomposing CO₂ fluxes measured over a mixed ecosystem at a tall tower and extending to a region: A case study, *J. Geophys. Res.*, *111*, G02005, doi:10.1029/2005JG000093.
- Wang, J. W., A. S. Denning, L. X. Lu, I. T. Baker, K. D. Corbin, and K. J. Davis (2007a), Observations and simulations of synoptic, regional, and local variations in atmospheric CO₂, *J. Geophys. Res.*, *112*, D04108, doi:10.1029/2006JD007410.
- Wang, W. G., K. J. Davis, B. D. Cook, C. X. Yi, M. P. Butler, D. M. Ricciuto, and P. S. Bakwin (2007b), Estimating daytime CO₂ fluxes over a mixed forest from tall tower mixing ratio measurements, *J. Geophys. Res.*, *112*, D10308, doi:10.1029/2006JD007770.
- Wofsy, S. C., and R. C. Harriss (2002), The North American Carbon Program (NACP), Report of the NACP Committee of the U.S. Interagency Carbon Cycle Science Program, 56 pp., U.S. Global Change Res. Program, Washington, D.C.
- Wofsy, S. C., M. L. Goulden, J. W. Munger, S.-M. Fan, P. S. Bakwin, B. C. Daube, S. L. Bassow, and F. A. Bazzaz (1993), Net exchange of CO₂ in a midlatitude forest, *Science*, *260*, 1314–1317.
- Xiao, X., S. Boles, J. Y. Liu, D. F. Zhuang, and M. L. Liu (2002), Characterization of forest types in Northeastern China, using multi-temporal SPOT-4 VEGETATION sensor data, *Remote Sens. Environ.*, *82*, 335–348.
- Xiao, X., D. Hollinger, J. Aber, M. Goltz, E. A. Davidson, Q. Zhang, and B. Moore III (2004a), Satellite-based modeling of gross primary production in an evergreen needleleaf forest, *Remote Sens. Environ.*, *89*, 519–534.
- Xiao, X., Q. Zhang, B. Braswell, S. Urbanski, S. Boles, S. C. Wofsy, B. Moore III, and D. Ojima (2004b), Modeling gross primary production of temperate deciduous broadleaf forest using satellite images and climate data, *Remote Sens. Environ.*, *91*, 256–270.
- Xiao, X., Q. Zhang, S. Saleska, L. Hutyrá, P. D. Camargo, S. C. Wofsy, S. Frolking, S. Boles, M. Keller, and B. Moore III (2005), Satellite-based modeling of gross primary production in a seasonally moist tropical evergreen forest, *Remote Sens. Environ.*, *94*, 105–122.
- Xu, L., and D. D. Baldocchi (2003), Seasonal trends in photosynthetic parameters and stomatal conductance of blue oak (*Quercus douglasii*) under prolonged summer drought and high temperature, *Tree Physiol.*, *23*(13), 865–877.
- Xu, L., and D. D. Baldocchi (2004), Seasonal variation in carbon dioxide exchange over a Mediterranean annual grassland in California, *Agric. For. Meteorol.*, *123*, 79–96.
- Yi, C., et al. (2004), A nonparametric method for separating photosynthesis and respiration components in CO₂ flux measurements, *Geophys. Res. Lett.*, *31*, L17107, doi:10.1029/2004GL020490.

V. Y. Chow, A. L. Dunn, E. W. Gottlieb, P. Mahadevan, J. W. Munger, and S. C. Wofsy, Department of Earth and Planetary Science and Division of Applied Science and Engineering, Harvard University, Cambridge, MA 02138, USA. (swofsy@deas.harvard.edu)

C. Gerbig, Max-Planck-Institut für Biogeochemie, Hans-Knoell-Straße 10, D-07745, Jena, Germany.

J. C. Lin, Department of Earth and Environmental Sciences, University of Waterloo, 200 University Avenue West, Waterloo, ON, N2L 3G1, Canada.

D. M. Matross, Department of Environmental Science, Policy, and Management, University of California, Berkeley, Berkeley, CA 94720, USA. (dmatross@nature.berkeley.edu)

X. Xiao, Complex Systems Research Center, Institute for the Study of Earth, Oceans and Space, Morse Hall, 39 College Road, University of New Hampshire, Durham, NH 03824, USA.